Continuous Changes in the Inner Order of the Crystalline Lamellae during Isothermal Crystallization of Poly(ϵ-caprolactone)

P. Kohn and G. Strobl*

Physikalisches Institut, Albert-Ludwigs-Universität, 79104 Freiburg, Germany

Received May 18, 2004; Revised Manuscript Received June 17, 2004

ABSTRACT: Simultaneous time-dependent small-angle and wide-angle X-ray scattering experiments (SWAXS) can be used to detect changes in the inner order of the lamellae growing during polymer crystallization. In SWAXS studies of crystallizing poly(ϵ-caprolactone) a delay in the development of the Bragg peaks relative to the increase of the Porod coefficient was detected. As indicated by the WAXS patterns, the weakening of the Bragg peaks is caused by innercrystalline disorder, which decreases with time.

1. Introduction

If polymers are heated after an isothermal crystallization, melting sets in immediately above the crystallization temperature, then increases in rate, and finally reaches a maximum near the end of the melting range. The extension of melting over a broad range is indicative for large variations in the stability of the crystallites. It appears that the first melting crystallites remain in an initial, lower ordered state, while those which persist until the end experience a maximum amount of stabilization. What is the mechanism of stabilization? The first suggestion came from Hoffman and Weeks,[1] who assumed that crystallites thicken after their first formation and in this way increase their stability. The view was accepted by many workers for a long time; however, it was finally contradicted by experiments. Correlation functions derived from SAXS curves measured during isothermal crystallization processes indicate generally a constant crystal thickness throughout the full crystallization time.[2−4] Hence, other explanations are required, and it is not difficult to provide them. Stability variations could originate also from the following: variations in the excess free energy associated with the fold surfaces, or intralamellar disorder of homogeneous or heterogeneous character, i.e., from perturbations of the crystal lattice or a crystalline−amorphous substructure.

Hints on the existence of intracrystalline disorder indeed came from vibrational spectroscopy. Hsu et al. in a work on functionalized polymethylene chains[5] detected a time delay between the chain stretching and the formation of hydrogen bonds. Yan et al. in an IR study of the crystallization of polypropylene[6] observed a sequential appearance of bands associated with an increasing length of ordered sequences. X-ray scattering experiments also have the potential to detect ordering processes within growing lamellae. Recently we started to use a camera for simultaneous small-angle and wide-angle X-ray scattering experiments (SWAXS). While small-angle X-ray scattering (SAXS) is based on the electron density difference between lamellae and melt independent of the inner structure of the lamellae, the Bragg reflections in the wide-angle scattering (WAXS) originate from crystal lattices only. Therefore, comparing the time dependencies of a convenient parameter of the SAXS curve and of the intensity of a Bragg reflection allows one to check whether the intralamellar order changes during the solidification process. We carried out such investigations on poly(ϵ-caprolactone) (PϵCL). In a previous study we reported the dependence of the crystal thickness d_c on the crystallization temperature T_c, and the Gibbs−Thomson relation between d_c and the melting point T_f.[3] Now, on the basis of SWAXS data, it will be shown that the order in crystallites of PϵCL improves continuously during the crystallization process.

2. Experimental Section

2.1. Samples. Experiments were carried out on samples of poly(ϵ-caprolactone) purchased from Aldrich Chemical Co. The molar mass was $M_n = 42.500$ ($M_w/M_n = 1.5$).

2.2. Simultaneous Small- and Wide-Angle X-ray Scattering. The X-ray scattering experiments were conducted with the aid of a twin camera produced by Hecus-M.Braun Co., Graz, Austria. In this device, a Kratky small-angle camera is complemented by a second camera which simultaneously registers the X-ray scattering in the angular range $2\theta = 19-26°$ (θ: Bragg scattering angle). Small-angle and wide-angle X-ray scattering curves are registered separately, employing two one-dimensional position-sensitive wire detectors. The intensity data obtained are stored and further evaluated in a PC. We used a Cu anode, fabricated by Bruker AXS, Karlsruhe, Germany, as the X-ray source, together with a Ni-filter to extract the Kα radiation.

2.2.1. Evaluation of SAXS Data. Having determined the primary beam intensity with the aid of a moving slit system, desmeared scattering curves were obtained in absolute values, as differential cross sections per unit volume $\Sigma(q)$. With a knowledge of $\Sigma(q)$, the one-dimensional electron density autocorrelation function $K(z)$ and its second derivative $K''(z)$, which gives the interface distance distribution function,[7,2] can be directly calculated by applying the Fourier relations

$$K(z) = \frac{1}{r_e^2}\frac{1}{(2\pi)^3}\int_0^\infty \cos qz \cdot 4\pi q^2 \Sigma(q)\, dq \qquad (1)$$

and

$$K''(z) = \frac{2}{r_e^2(2\pi)^2}\int_0^\infty [\lim_{q\to\infty} q^4\Sigma(q) - q^4\Sigma(q)]\cos qz\, dq \qquad (2)$$

Here, q denotes the scattering vector $q = 2\pi s = 4\pi \sin\theta/\lambda$; r_e is the classical electron radius.

* Corresponding author.

10.1021/ma049022m CCC: $27.50
Published on Web 08/07/2004

A useful parameter in kinetical measurements is the Porod coefficient. It generally describes for two phase systems the asymptotic behavior of the scattering curve as

$$\lim_{q\to\infty}\Sigma(q) = r_e^2\frac{P}{(q/2\pi)^4} \tag{3}$$

The Porod coefficient P is directly related to the interface area per unit volume, O_{ac}, by

$$P = \frac{1}{8\pi^3}O_{ac}(\Delta\eta)^2 \tag{4}$$

whereby $\Delta\eta$ denotes the difference in the electron densities of the two phases. This relation is generally valid for homogeneous as well as heterogeneous structures and therefore, for example, also if spherulites or other objects fill a sample only partially.

2.2.2. Determination of Bragg Reflection Intensities. The aim of the WAXS experiments was the determination of the intensities of Bragg reflections during structure-evolution and -modification processes, as they take place during isothermal crystallizations. We chose for PϵCL the 200-reflection, located at θ = 11.9°, together with an adjacent weaker reflection. In the first step, the WAXS curve of the melt—extrapolated to the crystallization temperature in order to account for the temperature shift of the halo, and adjusted to the measured curve—was subtracted from the data. Then the integral intensity I_B of the peak was determined.

2.2.3 The SWAXS Ratio. Small-angle X-ray scattering generally arises if densified regions with mesoscopic lengths exist in a sample, whereas Bragg reflections in the WAXS pattern occur only if crystals exist. If the solidification of a polymer after cooling a melt to a certain crystallization temperature takes place associated with the formation of crystal lamellae only, the development of scattering in the small-angle range and the scattering in the wide-angle range are directly related. More accurately, crystallinities may be derived from both WAXS and SAXS according to

$$\phi(\text{WAXS}) \sim I_B \tag{5}$$

and

$$\phi(\text{SAXS}) = \frac{O_{ac}d_c}{2} \sim Pd_c \tag{6}$$

If the solidification is due to crystal formation only, both should agree and the parameter

$$\alpha = \frac{I_B}{Pd_c} \tag{7}$$

addressed in the following as the SWAXS ratio, should be constant throughout the structure formation process. On the other hand, if the solidification is achieved by the growth of layers with a changing inner degree of order, variations in the value of the SWAXS ratio will occur.

2.3. Time-Dependent WAXS. WAXS curves over a larger angular range and their changes during the crystallization process were registered in a time-dependent measurement at the European Synchrotron Radiation Facility (ESRF) in Grenoble, France, using beamline BM26 (the wavelength is λ = 1.24 Å). Scattering curves were obtained within 30s with the aid of a 1D detector. Figure 1 shows as an example a series of curves obtained during an isothermal crystallization at 48 °C.

2.4. Dilatometry. Structure formation was also studied with the aid of a mercury filled dilatometer. Absolute values of the change in the specific volume were obtained after a calibration.

3. Results and Discussion

3.1. Structures at the End of Isothermal Crystallizations. PϵCL was isothermally crystallized at T_c = 48, 50, and 52 °C. To erase memory effects, samples were at first kept for 20 min in the melt at 130 °C before a rapid cooling to T_c. Crystallinities of PϵCL as given in the literature vary between 40 and 60%. Under these conditions it is impossible to derive the crystal thickness from the SAXS curve only. The best complementary measurement is an additional determination of the density change resulting from the crystallization, and we achieved that with the aid of a dilatometer.

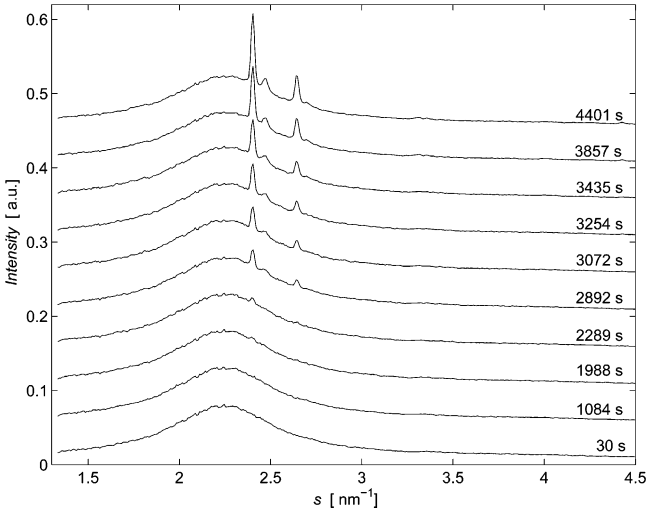

Figure 1. PϵCL, crystallization at 48 °C. Series of WAXS curves measured at ESRF, Grenoble, France (beamline BM26).

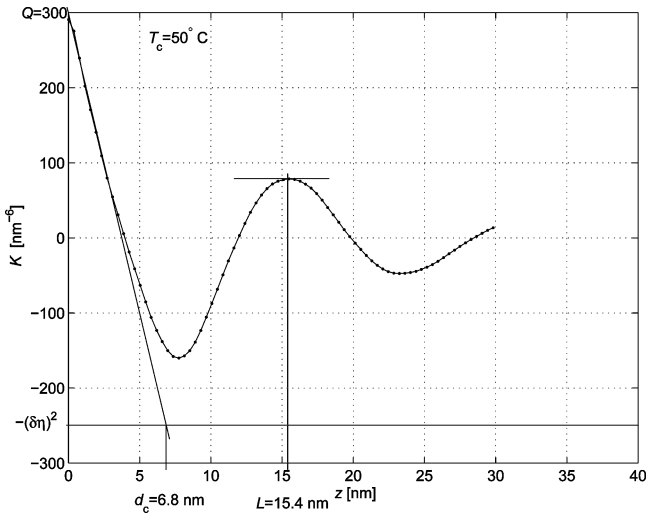

Figure 2. PϵCL, crystallized at 50 °C. Correlation function $K(z)$ derived from the SAXS curve together with the baseline following from the dilatometrically determined change in the mean electron density $\delta\eta$ = 15.8 nm^{-3}. The values of the crystal thickness d_c and the long spacing L are indicated.

Figure 2 refers to a measurement carried out at the end of an isothermal crystallization at 50 °C. The correlation function $K(z)$ was derived from the SAXS curve by a Fourier transformation according to eq 1. The baseline which is included in the figure was obtained by dilatometry. The change of the mean density, $\delta\rho$, follows from the measured change of the specific volume, δv, as

$$\delta\rho \approx \rho^2\delta v \tag{8}$$

where ρ = 1.02 g cm^{-3} denotes the melt density at 50 °C. The related change in the mean electron density is given by

$$\delta\eta = \delta\rho \frac{N_A \sum_i Z_i}{\sum_i A_i} \tag{9}$$

Knowing $\delta\eta$, the baseline, which is located at $-(\delta\eta)^2$ (compare with ref 8), can be introduced into the figure. The "self-correlation triangle", which is the representative of the crystal lamellae in $K(z)$, is sitting on the baseline and can therefore be constructed by a continuation of the linear initial part of $K(z)$ starting at $z = 0$. The crystal thickness, d_c, is given by the base length of the triangle. Here, it has a value of 6.8 nm. The crystallinity ϕ_c follows from

$$\phi_c = \frac{(\delta\eta)^2}{Q + (\delta\eta)^2} \tag{10}$$

leading to a value of 0.45. The density difference $\Delta\eta$ between the lamellae and the melt is given by

$$\Delta\eta = \frac{Q + (\delta\eta)^2}{\delta\eta} \tag{11}$$

which yields a value of 35 nm^{-3}.

Table 1 collects all data thus obtained for the structures formed after isothermal crystallizations at the three chosen temperatures. While the crystal thickness and also the long spacing increase by about 10%, the crystallinity remains unchanged at 0.45−0.46. The linear crystallinity $\phi_l = d_c/L$ is in good agreement with the overall crystallinity ϕ_c. This comes as expected for this sample, since it is completely filled with spherulites.

Approximate values for the crystallinities can also be derived from the decrease of the intensity I_H of the amorphous halo resulting from the crystallization. The equation

$$\phi_c' = 1 - \frac{I_H(t \to \infty)}{I_H(t = 0)} \tag{12}$$

provides an approximate value. It is less accurate than ϕ_c because crystals not only produce Bragg reflections but give also some contribution to the diffuse scattering. Values for ϕ_c' are also included in the table. As ϕ_c and ϕ_l, they are independent of the crystallization temperature. The value obtained, 0.42−0.43, is slightly smaller than the SAXS result, which could indeed be due to the diffuse scattering of the crystals.

3.2. Structure Development. Figure 3 depicts isotherms obtained by SWAXS experiments at the three different T_cs. They refer to the time dependence of the Porod coefficient P and the Bragg reflection intensity I_B. Porod coefficients were determined in absolute units, the Bragg reflection intensities are relative values obtained after an adjustment of P and I_B to equal end values. Comparing $P(t)$ and $I_B(t)$, a difference in the time dependence is noted. Compared to the Porod coefficient there is a distinct delay in the development of the Bragg reflection intensity. The difference can be expressed using the ratio α introduced in eq 7, and Figure 4 presents the time dependence of this quantity. There is a continuous increase with time, and this is indicative of an ongoing ordering process within the lamellae.

Support for an ordering process comes also from an evaluation of WAXS curves. During an isothermal

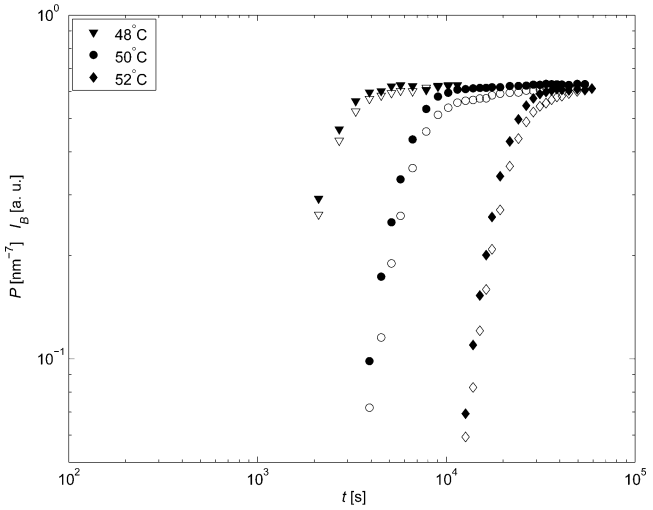

Figure 3. Isothermal crystallization at the indicated T_cs as observed by simultaneous small-angle and wide-angle X-ray scattering. Time dependence of the Porod coefficient P (filled symbols) and of the intensity I_B of Bragg reflections (open symbols).

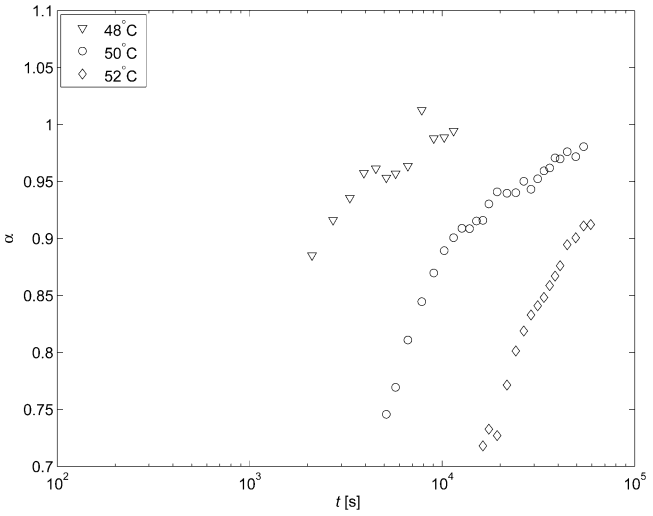

Figure 4. Isothermal crystallization at the indicated T_cs. Time dependence of the ratio $\alpha = I_B/(Pd_c)$ which characterizes the degree of order in the lamellae.

Table 1. Structure Parameters of PϵCL after a Crystallization at Three Different Temperatures T_c: Lamellar Thickness d_c, Long Spacing L, Linear Crystallinity $\phi_l = d_c/L$, Crystallinity ϕ_c Derived from SAXS and Dilatometry, Crystallinity ϕ_c' Derived from the Intensity Decrease of the Amorphous Halo, and Electron Density difference $\Delta\eta$ between Crystalline and Amorphous Regions

T_c (°C)	48	50	52
d_c (nm)	6.6	6.8	7.2
L (nm)	15.0	15.7	16.1
Φ_l	0.44	0.44	0.45
Φ_c	0.46	0.45	0.46
Φ_c'	0.43	0.42	0.42
$\Delta\eta$ (nm^{-3})	35	35	35

crystallization a series of curves was registered with the aid of a WAXS camera. Figure 5 presents one of the curves together with an adjusted scattering curve of the melt. The latter was obtained in its initial form at the begin of the measurements when the sample was still fluid and was then fitted to the curve obtained in the semicrystalline state. To remain below the actual curve everywhere, the scattering curve of the melt has to be

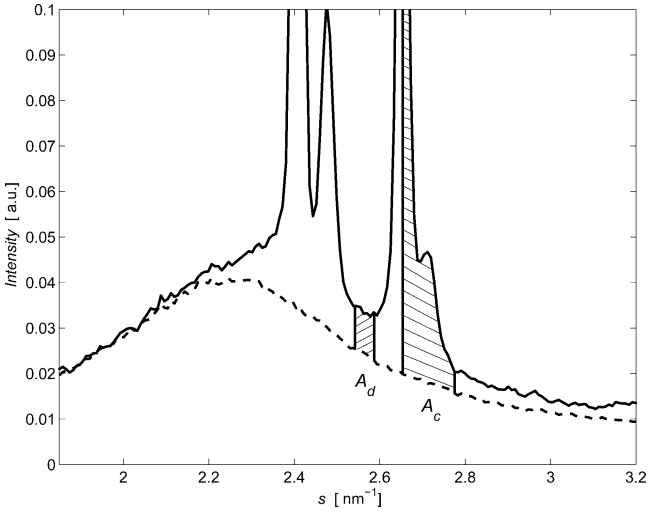

Figure 5. Wide-angle X-ray scattering curve with adjusted halo showing two selected ranges which are associated with diffuse scattering (area A_d) and Bragg scattering (area A_c), respectively. The ratio $\beta = A_c/A_d$ can serve as a measure of the intracrystalline order.

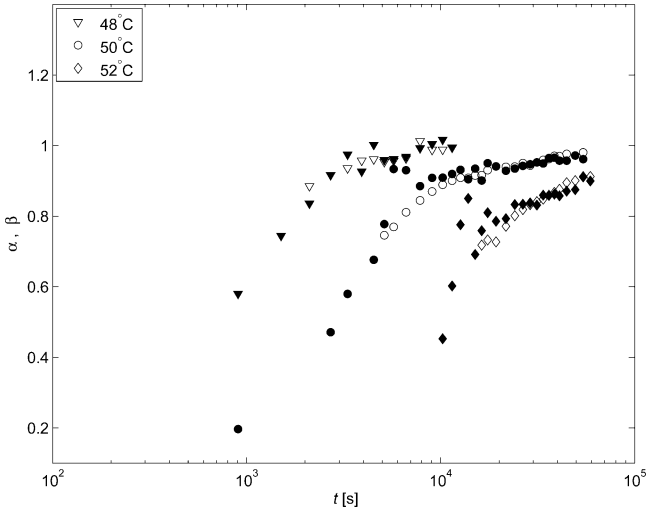

Figure 6. Isothermal crystallization at the indicated T_cs. Comparison between the time dependencies of α (open symbols) and β (filled symbols).

adjusted in the low-angle region. The fit demonstrates that the crystallites produce at higher angles some diffuse scattering, which means that they are disordered or imperfect. As it appears, the base part of the reflections is broadened which is—generally speaking—indicative for spatially correlated perturbations. We selected two angular ranges, one with diffuse scattering only and another at the position of two Bragg reflections, as is indicated in the figure. The integral intensities A_d and A_c within these two ranges allow to calculate the ratio

$$\beta = \frac{A_c}{A_d} \tag{13}$$

It can serve as a measure for the degree of order within the crystals. β is shown in Figure 6 as a function of time, in a comparison with the time dependence of α. Obviously both parameters show similar tendencies, with an even larger change showing up in β. Hence, both the time dependence of α and of β indicate that crystals in the initial stage of the formation are perturbed and then continuously improve their order. At the beginning, we asked about the mechanism of the stabilization process showing up in the difference between the crystallization temperature and the melting point. The ordering process going on within the lamellae of PϵCL has the potential to become a major contribution.

Acknowledgment. Support of this work by the Deutsche Forschungsgemeinschaft is gratefully acknowledged. Thanks are also due to the Fonds der Chemischen Industrie for financial help.

References and Notes

(1) Hoffman, J. D.; Weeks, J. J. *J. Res. Natl. Bur. Stand., Sect. A* **1962**, *66*, 13.
(2) Schmidtke, J.; Strobl, G.; Thurn-Albrecht, T. *Macromolecules* **1997**, *30*, 5804.
(3) Heck, B.; Hugel, T.; Iijima, M.; Sadiku, E.; Strobl, G. *New J. Phys. (Paris)* **1999**, *1*, 17.
(4) Rabiej, S.; Goderis, B.; Janicki, J.; Mathot, V. B. F.; Koch, M. H. J.; Groeninckx, G.; Reynaers, H.; Gelan, J.; Wlochowicz, A. *Polymer* **2004**, in press.
(5) Heintz, A. M.; McKiernan, R. L.; Gido, S. P.; Penelle, J.; Hsu, S. L. *Macromolecules* **2002**, *35*, 3117.
(6) Zhu, X. Y.; Yan, D. Y.; Fang, Y. P. *J. Phys. Chem.* **2001**, *105*, 12461.
(7) Ruland, W. *Colloid Polym. Sci.* **1977**, *255*, 417.
(8) Strobl, G. *The Physics of Polymers*; Springer: Berlin, 1997; p 408.

MA049022M